



OPEN

Nitrogen concentration driving the hardness of rhenium nitrides

SUBJECT AREAS:

CONDENSED-MATTER
PHYSICS

CHEMICAL PHYSICS

Zhonglong Zhao, Kuo Bao, Da Li, Defang Duan, Fubo Tian, Xilian Jin, Changbo Chen, Xiaoli Huang, Bingbing Liu & Tian Cui

State Key Laboratory of Superhard Materials, College of physics, Jilin University, Changchun, 130012, P. R. China.

Received

26 February 2014

Accepted

8 April 2014

Published

25 April 2014

Correspondence and
requests for materials
should be addressed to
T.C. (cuitian@jlu.edu.
cn)

The structures and properties of rhenium nitrides are studied with density function based first principle method. New candidate ground states or high-pressure phases at Re:N ratios of 3 : 2, 1 : 3, and 1 : 4 are identified via a series of evolutionary structure searches. We find that the 3D polyhedral stacking with strong covalent N-N and Re-N bonding could stabilize Re nitrides to form nitrogen rich phases, meanwhile, remarkably improve the mechanical performance than that of sub-nitrides, as Re_3N , Re_2N , and Re_3N_2 . By evaluating the trends of the crystal configuration, electronic structure, elastic properties, and hardness as a function of the N concentration, we proves that the N content is the key factor affecting the metallicity and hardness of Re nitrides.

The combination of electron-rich $4d$ and $5d$ transition metals (TM) with light covalent-bond forming elements (LE) like B, C, N, and O has been proved to be an effective way to design novel superhard material over the past decade^{1–3}. The idea is that the collaboration of TM's high electron concentration (EC) and the directional bonding formed by strong hybridizations between TM d electrons and LE s, p electrons can effectively withstand both elastic and plastic deformations. With this philosophy, compounds such as OsB_2 ⁴, ReB_2 ⁵, PtN_2 ^{6,7}, IrN_2 ^{7,8}, OsN_2 ⁸, and PdN_2 ⁹ were successfully designed. All of them are promising candidates for superhard and fracture-resistant materials with the elastic modulus comparable to diamond and c -BN. Recently, two Re sub-nitrides Re_3N (SG $P-6m2$) and Re_2N (SG $P6_3/mmc$) were synthesized by Friedrich *et al.*¹⁰ at moderate pressures (13–20 GPa) and temperatures (1600–2400 K). The ultra-high bulk modulus of > 400 GPa made them novel ultra-incompressible materials^{10–17}. However, independent theoretical works by Zhang *et al.*¹⁸ and Zang *et al.*¹⁹ proved that the relatively lower ideal tensile strengths inherently limit the application of Re_3N and Re_2N as superhard material. This discrepancy tells that the small compressibility is not equal to high hardness²⁰, and the high EC of Re sub-nitrides which is responsible for their low compressibility should actually go against the directional bonding. The Re:N stoichiometry may be the key to understand the competition between the EC and the directional bonding. And recent experimental and theoretical attempts to design N-rich Re nitrides are the subjects of intensive interest. Zhao *et al.*²¹ and Wang *et al.*²² proposed that Re mononitride forms in wurtzite-type, NbO-type, and NiAs-type structures, respectively. Besides, orthorhombic (SG $Pbcn$) and tetragonal (SG $P4/mmm$) Re dinitrides (denoted as orth- ReN_2 and tetr- ReN_2) with high bulk and shear modulus has been predicted theoretically^{23–25}. Recently, Kawamura *et al.*²⁶ synthesized the MoS_2 -type ReN_2 with metathesis reaction. However, the MoS_2 -type ReN_2 with a weak bulk modulus is less stable according to the calculations of Wang *et al.*²⁷, and a monoclinic structure (SG $C2/m$) was proposed. In addition, the hypothetical ReP_4 -type ReN_4 with high computational hardness has also been predicted by Zhao *et al.*²⁸ and Aydin *et al.*²⁹.

Despite the substantial amount of works focused on Re nitrides. There are still two questions to be answered. Firstly, the multiple oxidation states of Re promise the emergence of Re-N phases at wide stoichiometries and pressures. Therefore a comprehensive study to update the Re-N phase diagram toward different Re/N ratios and pressures, especially in the N-rich side, is necessary. Secondly, the effect of the N concentration on the mechanical behavior of Re nitrides and relevant mechanism are still unclear. To address these issues, we employ a series of evolutionary structure searches to reconstruct the low- T Re-N phase diagram at moderate pressures of 0–100 GPa. New stable phases for the known Re:N ratios and new stoichiometries were updated and established. The trends of the crystal structure, electronic transition, and mechanical performance of Re nitrides as a function of N concentration are compared based on the updated full-scale Re-N phase diagram. The results show that the metallicity and hardness of Re nitrides can be correlated to the N content, and N-rich Re nitrides are better candidates for superhard materials due to the strong 3D covalent structural networks.



Table 1 | Space group (SG); calculated lattice parameters, a , b , and c (Å); unit cell volume V_0 (Å³); and formation energy E_f (eV/atom) of Re, Re₃N, Re₂N, Re₃N₂, ReN₂, and ReN₃ at 0 GPa. And the parameters of high- P phase ReN₄ at 50 GPa

Phase		SG	a	b	c	V_0	E_f
Re	This work	$P6_3/mmc$	2.77		4.48	14.93	
	Ref. 38		2.76		4.46		
Re ₃ N	This work	$P-6m2$	2.83		7.16	49.74	-0.03
	Ref. 10		2.78		7.15		
	Ref. 18		2.83		7.19		
Re ₂ N	This work	$P6_3/mmc$	2.86		9.87	34.89	0.03
	Ref. 10		2.83		9.88		
	Ref. 18		2.86		9.88		
Re ₃ N ₂	This work	$P-6m2$	2.84		8.30	57.94	-0.03
ReN ₂	This work	$C2/m$	6.83	2.84	9.39	27.77	0.19
	Ref. 27		6.82	2.84	9.36		
ReN ₃	This work	$Imm2$	5.25	2.81	4.75	34.97	0.44
ReN ₄	This work	$Cmmm$	7.54	3.59	2.63	35.50	0.83

Results and discussion

The global stability of Re nitrides can be quantified by constructing the thermodynamic convex hull within considered pressures, which is defined as the average atom formation enthalpy of the most stable phases at each composition: $\Delta H = H(\text{Re}_x\text{N}_y) - xH(\text{Re}) - yH(\text{N}_2)/2$. Any structure with the enthalpy lies on the convex hull is considered to be thermodynamically stable and synthesizable experimentally^{30–32}. To give a more realistic prediction, both the experimental³³ and computational^{34,35} high- P (low- T) phase orders of nitrogen were adopted (the ζ -N₂ was replaced by ε -N₂ in the calculations due to its structural uncertainty). The formation energy E_f of predicted Re

nitrides can be calculated in the same way, listed in Table 1. The high-pressure convex hull and pressure-composition phase diagram of Re nitrides are depicted in Figure 1 and Figure 2. We present a rich phase content of Re nitrides toward different Re:N ratios and pressures. Particularly, three stable phases denoted as $P-6m2$ -Re₃N₂, $Imm2$ -ReN₃, and $Cmmm$ -ReN₄, beside the well-known Re₃N, Re₂N sub-nitrides, and N-rich ReN₂, are proposed here as the complements to the Re-N phase diagram. It follows that the formation of Re nitrides, especially in the N-rich side, will be endothermic processes at absolute 0 K and 0 GPa due to their positive formation energies toward the thermodynamic summation of Re and α -N₂.

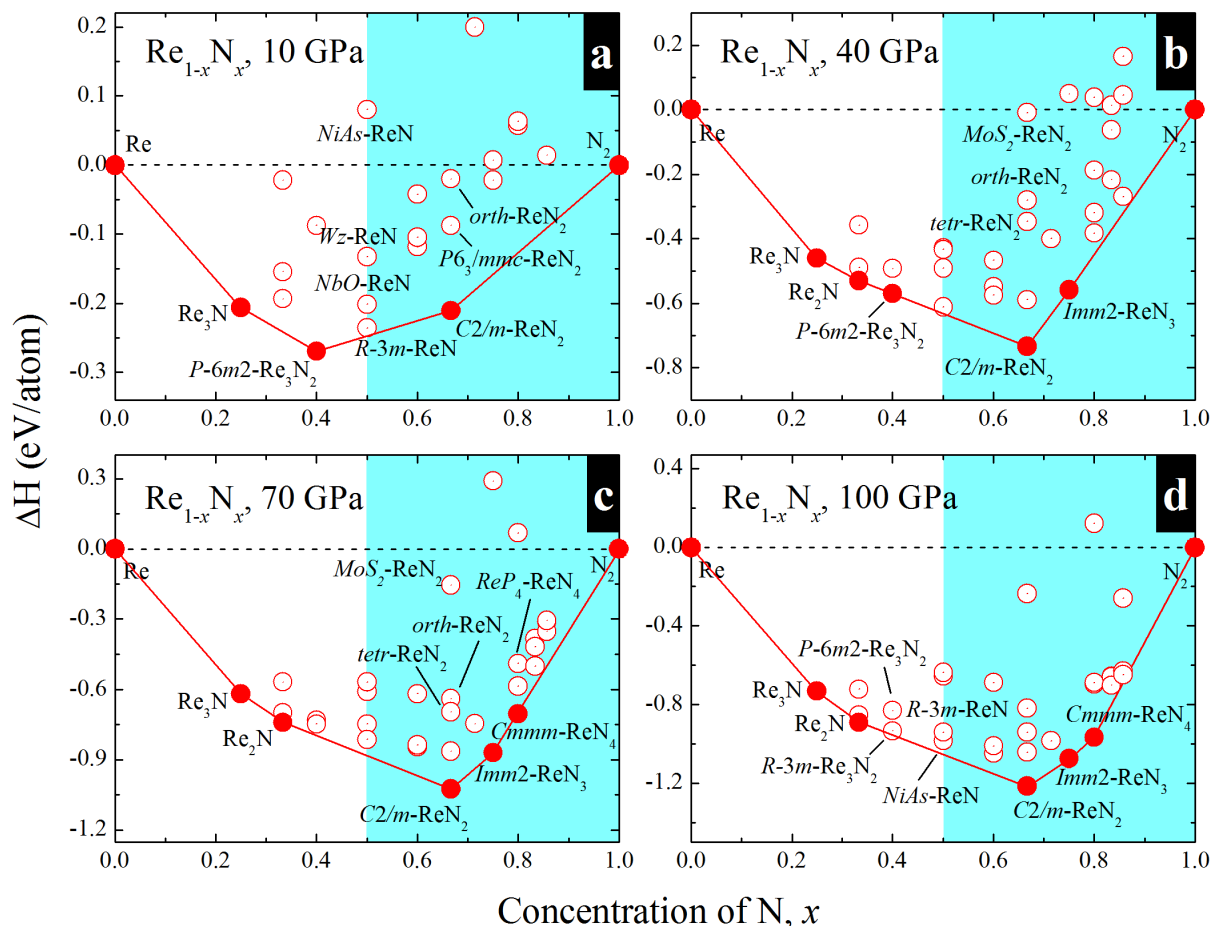


Figure 1 | Convex hull diagram for Re-N system. At pressures of (a) 10 GPa, (b) 40 GPa, (c) 70 GPa, and (d) 100 GPa, respectively. Solid circles represent stable phases while open circles denote metastable phases. N-rich stoichiometries are highlighted by cyan shadows.

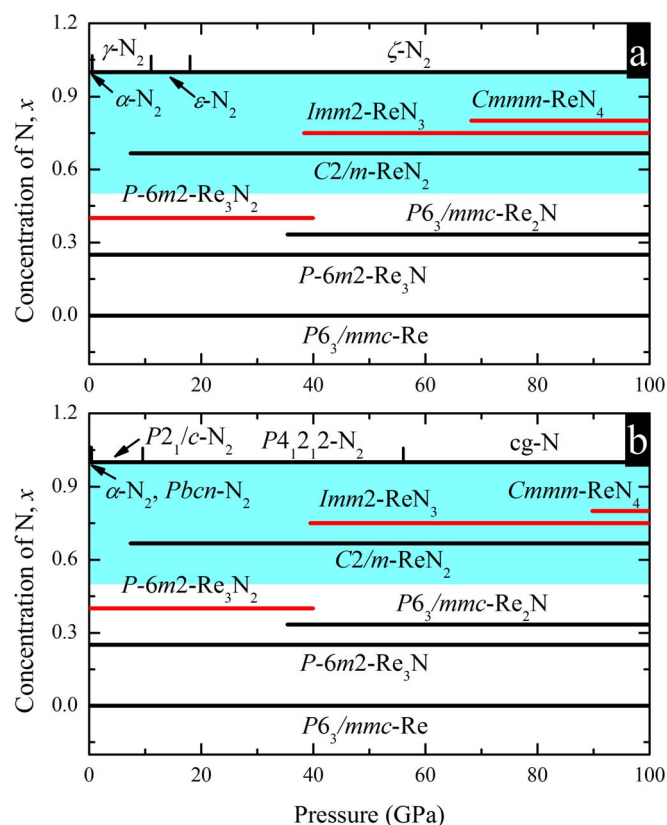


Figure 2 | Pressure-composition phase diagram for Re-N system.

Calculated with the (a) experimental (Ref. 33) and (b) computational (Ref. 34,35) phase orders of nitrogen, respectively. Red lines represent new phases proposed in this work. N-rich stoichiometries are highlighted by cyan shadows.

For Re sub-nitrides, Re_3N is stable at whole considered pressures while Re_2N is thermodynamically stable only at high pressures, which is accord with the experimental results of Friedrich *et al.*¹⁰ and make our thermodynamic calculations reliable. In addition to the experimental sub-nitrides, our structure searches establish the ground state of new Re_3N_2 stoichiometry for the first time (denoted as $P\text{-}6m2\text{-Re}_3\text{N}_2$), which is thermodynamically stable up to 40.0 GPa as shown in Figure 1 and Figure 2. For the N-rich side, structure searching confirms that the $C2/m\text{-ReN}_2$ proposed by Wang *et al.*²⁷ is the most stable phase and can be synthesized at the pressures of above 7.4 GPa. The previous orth- ReN_2 , tetra- ReN_2 , and MoS_2 -type ReN_2 ²⁶ become metastable phases during the considered pressures. With further increasing the N concentration, a new stable structure (denoted as $Imm2\text{-ReN}_3$) with extended Re:N ratio of 1:3 can be synthesized at wide pressures of 38.3–100 GPa (see Figure 2 (a)). And for Re tetranitrides, the proposed $Cm3m\text{-ReN}_4$ is stable at elevated pressures of above 68.2 GPa, which can be viewed as the limit of high N content phase of the predicted 0–100 GPa Re-N phase diagram. Note that the hypothetical $\text{ReP}_4\text{-ReN}_4$ predicted by Zhao *et al.*²⁸ and Aydin *et al.*²⁹ should also be a metastable phase and can hardly be synthesized (see Figure 1 (c)). The adoption of the computational high- P phase order of nitrogen^{34,35} gives consistent phase diagram of Re nitrides, displayed in Figure 2 (b), except that the stable pressures of $Imm2\text{-ReN}_3$ and $Cm3m\text{-ReN}_4$ have been raised to 39.5 and 89.8 GPa, respectively.

The crystal structures of Re nitrides are schematically showed in Figure 3. The mechanical and dynamical stabilities are examined by calculating the elastic constants (see Supplementary Table S1 online) and phonon dispersions (see Supplementary Figure S1 online), all proposed phases are mechanically stable at 0 GPa with the elastic

constants meet the Born-Huang stability criteria³⁶. Besides, the $P\text{-}6m2\text{-Re}_3\text{N}_2$ is dynamically stable at 0 GPa. And N-rich $C2/m\text{-ReN}_2$ and $Imm2\text{-ReN}_3$ are tested to be dynamically stable from 0 GPa to their synthetic pressures, which means that they are quenchable to the ambient condition. The $Cm3m\text{-ReN}_4$ is dynamically stable at high pressures (50–100 GPa). According to Figure 3, a unique structural transition induced by increasing N content can be clearly revealed. The Re-Re-N-Re, Re-N-Re, and Re-Re-N-N-Re lamellar stacking orders of Re_3N , Re_2N , and Re_3N_2 sub-nitrides has been broken and transformed into intriguing polyhedral stacking configurations as in $C2/m\text{-ReN}_2$, $Imm2\text{-ReN}_3$, and $Cm3m\text{-ReN}_4$. Among them, the structure of Re_3N_2 is special since it can be viewed as the substitution of the isolated N with N_2 dimer in the configuration of Re_3N . This reveals that the segregation of Re layers by N bilayer can stabilize Re nitride to low energy and also weak metallicity (see the following electronic structure discussions). With this idea, an analogous structure can be built for ReN that is by substituting the N with N_2 dimer in Re_2N along the c -axes. Along with slightly stagger of the neighbouring two Re layers, it results in $R\text{-}3m\text{-ReN}$, which is more stable than the wurtzite-ReN, NbO-ReN, and NiAs-ReN proposed by Zhao *et al.*²¹ and Wang *et al.*²² (see Figure 1 (a)), and can easily be obtained by the 1:1 fixed Re:N ratio evolutionary structure searches. However, the lamellar order with a growing number of the vertical N_2 dimers destabilize Re nitride. The $R\text{-}3m\text{-ReN}$ is metastable and will decompose into Re_3N_2 and ReN_2 as shown in Figure 1. Besides, the introduction of N_2 dimer can lower the crystal density and results in large volume phases. The PV works will sacrifice the enthalpies markedly, which is responsible for the instability of Re_3N_2 at high pressures. The polyhedral stacking configuration can be an effective way to stable Re nitride and forms in dense N-rich phases. For $C2/m\text{-ReN}_2$, the stacking consists of the corner or edge shared ReN_7 decahedrons and also bonded with N-N connections according to Figure 3 (e). With an additional N into the lattice, the stacking for $Imm2\text{-ReN}_3$ consists of more regular ReN_7 octahedrons with the connections of the special tri-nitrogen units (see Figure 3 (f)). As to the high-pressure phase $Cm3m\text{-ReN}_4$, the novel ReN_8 cubic box can actually be formed due to the coordination number of Re changing from 7 to 8. The parallel ~ 1.40 Å N-N bonds (0 GPa) in $C2/m\text{-ReN}_2$, $Imm2\text{-ReN}_3$, and $Cm3m\text{-ReN}_4$ represent the typical single N-N bond lengths in PM nitrides, e.g., 1.41 Å for PtN_2 , 1.43 Å for OsN_2 , and 1.42 Å for IrN_2 , therefore we can draw the conclusion that N-N forms in single bond since the bond-length similarity within a related bonding scheme³⁷. The common polyhedral stacking configurations of N-rich Re nitrides is a prerequisite for superhard since it can avoid the direct Re-Re interactions, and the structural networks can be constructed primarily by Re-N and N-N covalent bonds. The space group, calculated equilibrium lattice parameters, and the unit cell volumes of rhenium nitrides with various stoichiometries are listed in Table 1. Our calculated lattice parameters of Re, Re_3N , Re_2N , and $C2/m\text{-ReN}_2$ are all in good accordance with previous studies^{10,18,27,38}.

The updated full-scale Re-N phase diagram allows us to evaluate the trend of the mechanical performance of Re nitrides as the function of N concentration, and correlate it with the structural and electronic transitions. The calculated bulk modulus (B), shear modulus (G), Young's modulus (E), Poisson's ratios (ν), densities (ρ), and hardness (H_V) of Re nitrides at different N concentrations are depicted in Figure 4 and Table 2 (for comparability, the elastic data of the high- P phase $Cm3m\text{-ReN}_4$ in Figure 4 are achieved at 0 GPa), while the electronic density of states (DOS) are showed in Figure 5. Re nitrides have similar metallic bonding features owing to the finite DOS at the Fermi level (E_F), which originate mostly from $5d$ electrons of Re. According to Figure 4 (a) and (e), the high N content in the crystal can decline the bulk modulus and densities markedly, which heralds the decrease of the incompressibility and EC of N-rich Re nitrides. This is accords with the reducing of the metallicity, i.e., the

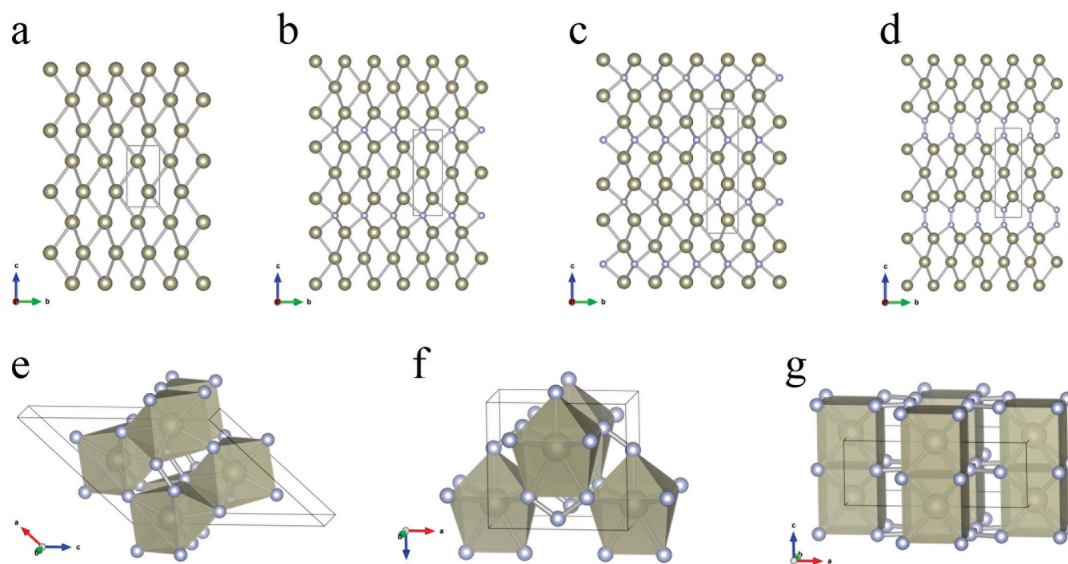


Figure 3 | Crystal structures of Re nitrides. (a) Re; (b) Re_3N ; (c) Re_2N ; (d) $P-6m2-\text{Re}_3\text{N}_2$: Re1 atoms occupy the $1f$ (0.6667, 0.3333, 0.5), Re2 atoms occupy the $2h$ (0.3333, 0.6667, 0.2361), and N atoms occupy the $2i$ (0.6667, 0.3333, 0.0841) positions; (e) $C2/m-\text{ReN}_2$; (f) $Imm2-\text{ReN}_3$: Re atoms occupy the $2b$ (0.5, 0, 0.3466), N1 atoms occupy the $4c$ (0.21, 0.5, 0.2455), and N2 atoms occupy the $2b$ (0, 0.5, 0.4123) positions; and (g) $Cmmm-\text{ReN}_4$ (at 50 GPa): Re atoms occupy the $2b$ (0, 0.5, 0), while N atoms occupy the $8q$ (0.8401, 0.1927, 0.5) positions. Large and small balls denote Re and N atoms, respectively.

DOS at the Fermi level ($N(E_F)$), of Re nitrides at elevated N concentrations. Here, we should note that the $Imm2-\text{ReN}_3$ with the lowest B possess the $N(E_F)$ minimum of ~ 0.11 eV/atom (see Figure 5). On the other hand, a parallel increase of shear modulus, Young's modulus, and a reduction of Poisson's ratios can be clearly revealed with increasing N contents, as shown in Figure 5 (b), (c), and (d). The unsmooth change of the G , E , and ν between the Re_3N , Re_2N , and Re_3N_2 sub-nitrides can be attributed to the discontinuity of the C_{12} and C_{13} elastic constants (see Supplementary Table S1 online), which relate to the Poisson effect in the hexagonal structures. According to Table 2, the calculated mean value of the G and E for N-rich $C2/m-\text{ReN}_2$, $Imm2-\text{ReN}_3$, and $Cmmm-\text{ReN}_4$ are about 46 and 86 GPa respectively higher than that of Re and sub-nitrides. In addition, the Poisson's ratios of $Imm2-\text{ReN}_3$ and $Cmmm-\text{ReN}_4$ have been dropped down from the typically delocalized metals (~ 0.3) to the level of strong directional covalent materials (~ 0.2). The reinforcement of the N-rich Re nitrides has its own origin and can be attributed to the enhanced hybridizations between N $2p$ and Re $5d$ electronic states (i.e., in the bonding states of -5 to 0 eV below the Fermi level) as shown in Figure 5. Therefore, we can conclude that the primary contribution of the high N content to N-rich Re nitrides is that it facilitates more p electrons involved in bonding, thus can translate the material from high EC strong metal sub-nitrides to the strong covalent N-rich nitrides with enhanced directional bondings. These results suggest that the N content is a key factor to influence the hardness of Re nitrides and the hardness of $C2/m-\text{ReN}_2$, $Imm2-\text{ReN}_3$, and $Cmmm-\text{ReN}_4$ should be far higher than that of Re_3N , Re_2N , and Re_3N_2 sub-nitrides.

The hardness of Re nitrides as a function of N concentration is estimated by recently proposed empirical model³⁹ with the formula $H_V = 2.0(k^2G)^{0.585} - 3.0$, as shown in Figure 4 (f). It can be seen that the high N content promote the hardness of Re nitrides according with the changes of G , E , and ν as discussed above. On the other hand, the strong covalency of the bonding in N-rich Re nitrides allows us to evaluate their intrinsic hardness by microscopic hardness models^{40–43}. Here we use the method proposed by Gao *et al.*⁴⁰ and its further development which includes a small metallic component of chemical bond and considering the orbital form of $s-p$ or $s-p-d$ ⁴⁴. The

hardness of the μ -type particular bond in metallic and $s-p-d$ hybridized crystals is written as^{40,44,45}:

$$H_V^\mu(\text{GPa}) = A_0(N_e^\mu)^{2/3}(d^\mu)^{-2.5}e^{-1.191f_i^\mu - 32.2(f_m^\mu)^{0.55}} \quad (1)$$

where A_0 is the proportionality coefficient takes 350 and 1051 for the pure covalent N-N and polar covalent Re-N bonds, respectively. N_e is the valence electron density of the bond, d is the bond length. The Phillips ionicity f_i of chemical bond is calculated by the Mulliken population⁴⁶. The f_m in Equation (1) is a factor introduced to account for the metallicity effect on hardness and can be calculated as $f_m = k_B TD_F/n_e$, where n_e is the total number of valence electrons in the unit cell, D_F is the density of electronic states at the Fermi level⁴⁴. The total hardness can be expressed as the average of all bond hardnesses:

$$H_V = \left[\prod^\mu (H_V^\mu)^{n^\mu} \right]^{1/\sum n^\mu} \quad (2)$$

where n^μ is the number of bond of type μ composing the actual complex crystal. The detailed bond parameters of hardness calculations can be found as Supplementary Table S2 online. The hardness of $C2/m-\text{ReN}_2$ and $Imm2-\text{ReN}_3$ at ambient condition are evaluated as 38.4 and 44.4 GPa respectively, which could be potential candidates to be superhard materials.

Conclusion

In summary, we have systematically explored the structures and properties of Re nitrides at wide stoichiometries and pressures with *ab initio* evolutionary method. We corrected the stable structure of ReN_4 to the phase with the $Cmmm$ symmetry, and new stoichiometries of $P-6m2-\text{Re}_3\text{N}_2$ and $Imm2-\text{ReN}_3$ are established for possible synthesis. It is found that high-pressure can be an effective approach to stable Re nitrides. The $C2/m-\text{ReN}_2$, $Imm2-\text{ReN}_3$, and $Cmmm-\text{ReN}_4$ can be synthesized at pressures above 7.4, 38.3, and 68.2 GPa, respectively. And $C2/m-\text{ReN}_2$ and $Imm2-\text{ReN}_3$ are retainable to ambient condition. A good relation between the mechanical behavior and N concentration was established by detailed evaluating the variations of the crystal configurations, electronic structures, elastic properties, and computational hardness. Our

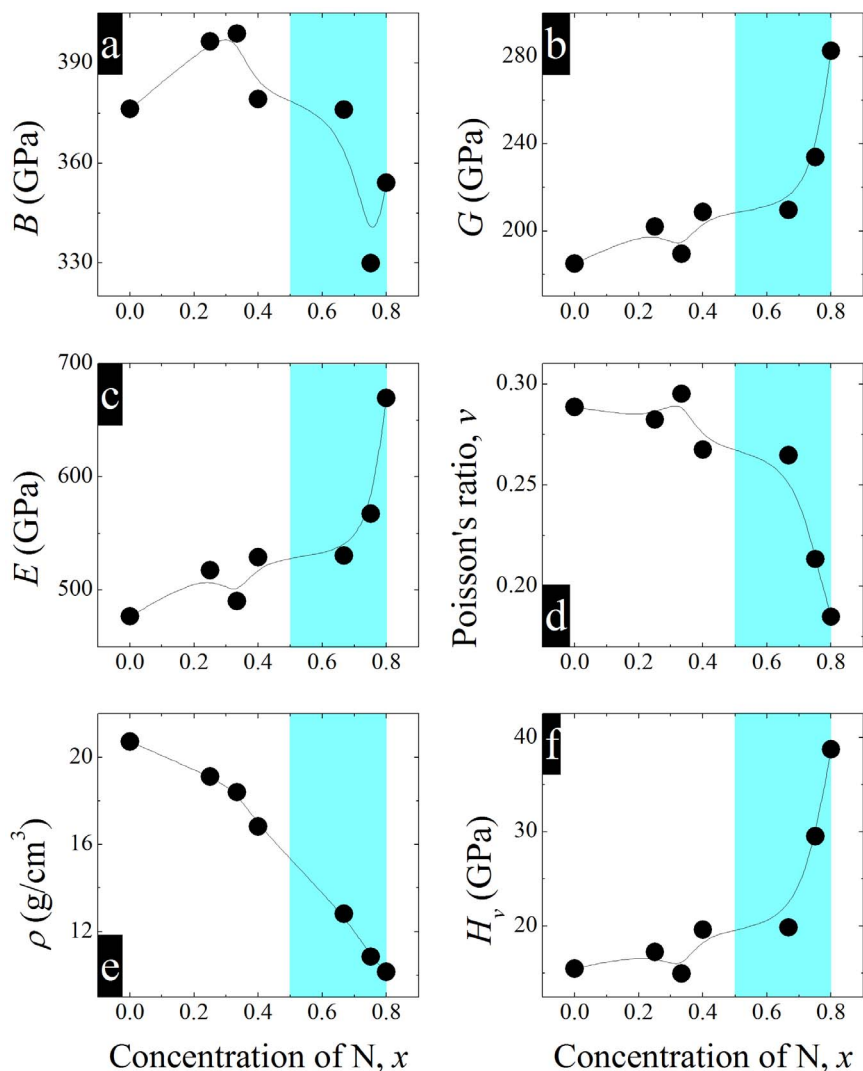


Figure 4 | Elastic properties of Re nitrides at 0 GPa. Calculated (a) bulk modulus B (GPa), (b) shear modulus G (GPa), (c) Young's modulus E (GPa), (d) Poisson's ratio ν , (e) density ρ (g/cm^3), and (f) Vickers hardness H_V (GPa) of Re nitrides as a function of N concentration. The neighboring data points were connected by B-Spline to evaluate the changing trends. N-rich stoichiometries are highlighted by cyan shadows.

results show that the high N content benefits the formation of the covalent 3D polyhedral stacking structure and can effectively avoid the weak Re-Re metal interactions, which result in the reinforcement of the Re nitrides from ultra-incompressible sub-nitrides to superhard N-rich materials. These results are expected to stimulate the exploration and discovery of new material, and the approach of

harden Re nitride by high LE content may also applicable to other TM compounds.

Methods

Evolutionary structure searches are performed with USPEX code^{47–49}. Structure cells with Re:N ratios of 3:1, 2:1, 1.5:1, 1:1, 1:1.5, 1:2, 1:2.5, 1:3, 1:4, 1:5, and 1:6

Table 2 | Calculated bulk modulus B (GPa), shear modulus G (GPa), Young's modulus E (GPa), Poisson's ratio ν , density ρ (g/cm^3), and Vickers hardness H_V (GPa) of Re-N system at different pressures

Phase		SG	P	B	G	E	ν	ρ	H_V
Re	This work	$P6_3/mmc$	0 GPa	376	185	477	0.29	20.72	15.49
Re ₃ N	This work	$P-6m2$	0 GPa	397	202	518	0.28	19.12	17.26
	Ref. 10			395					
	Ref. 18			397	203				
Re ₂ N	This work	$P6_3/mmc$	0 GPa	399	189	490	0.30	18.40	14.98
	Ref. 10			401					
	Ref. 18			401	182				
Re ₃ N ₂	This work	$P-6m2$	0 GPa	379	209	529	0.27	16.82	19.63
ReN ₂	This work	$C2/m$	0 GPa	376	210	531	0.26	12.81	19.86
	Ref. 27			369	217				
ReN ₃	This work	$Im\bar{m}2$	0 GPa	330	234	568	0.21	10.84	29.51
ReN ₄	This work	$Cmmm$	0 GPa	354	283	670	0.18	10.15	38.72
ReN ₄	This work	$Cmmm$	50 GPa	528	379	919	0.21	11.33	40.82

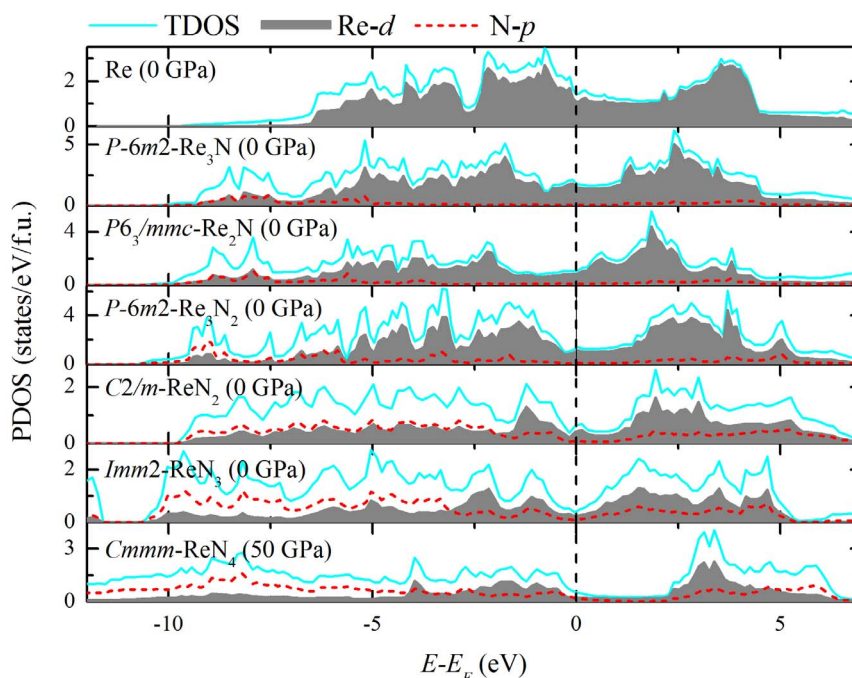


Figure 5 | Calculated total (TDOS) and partial density of states (PDOS) of Re nitrides at different pressures. The vertical dash line at zero is the Fermi energy level.

within 2 and 4 formula units (f.u.) are implemented at 0, 30, 60, and 100 GPa, respectively. To update a full-scale Re-N phase diagram, moreover, variable-composition structure predictions⁵⁰ are also performed at 0, 50, and 100 GPa, respectively. The first generation of structures was produced randomly and the succeeding generations were obtained by applying heredity (60%), atom transmutation (10%), and lattice mutation (30%) operations. Each structure was fully relaxed to an energy minimum at different pressures with the Vienna *ab initio* simulation package (VASP)⁵¹. The projector augmented waves (PAW) method⁵² within the generalized gradient approximation (GGA) of Perdew-Burke-Ernzerhof (PBE)⁵³ was adopted. By performing accurate convergence tests, we choose a cutoff of 520 eV for the wave function expansion into plane waves and a k -mesh of $0.03 \times 2\pi \text{ \AA}^{-1}$ within the Monkhorst-Pack scheme for sample the Brillouin zone, which ensures the error bars of total energies are less than 1 meV/atom. Besides, all forces on atoms were converged to less than 1 meV/Å and the total stress tensor was reduced to the order of 0.01 GPa. Phonon curves were calculated by the direct supercell method with the forces obtained by the Hellmann-Feynman theorem^{54,55}. Elastic constants were calculated by the strain-stress method, while bulk modulus B , shear modulus G , Young's modulus E , and Poisson's ratio ν are derived from the Voigt-Reuss-Hill averaging scheme⁵⁶. The theoretical Vickers hardness was estimated by using the Chen's model³⁹ and the Gao's model⁴⁰, respectively. For the latter, the Mulliken bond population is calculated with the CASTEP code^{57,58}. The ultra-soft Vanderbilt pseudopotential (USPP)⁵⁹ with PBE-GGA is chosen. The cutoff energy and k -mesh are same as the setting in VASP calculations.

- Brazhkin, V. V., Lyapin, A. G. & Hemley, R. J. Harder than diamond: Dreams and reality. *Philos. Mag. A* **82**, 231–253 (2002).
- Kaner, R. B., Gilman, J. J. & Tolbert, S. H. Designing Superhard Materials. *Science* **308**, 1268–1269 (2005).
- Chung, H.-Y. *et al.* Synthesis of Ultra-Incompressible Superhard Rhenium Diboride at Ambient Pressure. *Science* **316**, 436–439 (2007).
- Cumberland, R. W. *et al.* Osmium diboride, an ultra-incompressible, hard material. *J. Am. Chem. Soc.* **127**, 7264–7265 (2005).
- Chung, H.-Y. *et al.* Synthesis of ultra-incompressible superhard rhenium diboride at ambient pressure. *Science* **316**, 436–439 (2007).
- Gregoryanz, E. *et al.* Synthesis and characterization of a binary noble metal nitride. *Nat. Mater.* **3**, 294–297 (2004).
- Crowhurst, J. C. *et al.* Synthesis and Characterization of the Nitrides of Platinum and Iridium. *Science* **311**, 1275–1278 (2006).
- Young, A. F. *et al.* Synthesis of Novel Transition Metal Nitrides IrN₂ and OsN₂. *Phys. Rev. Lett.* **96**, 155501 (2006).
- Crowhurst, J. C. *et al.* Synthesis and characterization of nitrides of iridium and palladium. *J. Mater. Res.* **23**, 1–5 (2008).
- Friedrich, A. *et al.* Novel Rhenium Nitrides. *Phys. Rev. Lett.* **105**, 085504 (2010).
- Friedrich, A., Winkler, B., Refson, K. & Milman, V. Vibrational properties of Re₃N from experiment and theory. *Phys. Rev. B* **82**, 224106 (2010).

- Bannikov, V. V., Shein, I. R. & Ivanovskii, A. L. Elastic and electronic properties of hexagonal rhenium sub-nitrides Re₃N and Re₂N in comparison with hcp-Re and wurtzite-like rhenium mononitride ReN. *Phys. Status Solidi. B* **248**, 1369–1374 (2011).
- Hao, X. F. *et al.* Elastic properties of novel rhenium nitrides from first principles. *Phys. Status Solidi. B* **248**, 2107–2111 (2011).
- Deligoz, E., Colakoglu, K., Ozisik, H. B. & Ciftci, Y. O. Vibrational properties of Re₂N and Re₃N compounds. *Solid State Commun.* **151**, 1122–1127 (2011).
- Liang, Y. C., Yuan, X. & Zhang, W. Q. Ultrastiffness and metallicity of rhenium nitrides. *J. Appl. Phys.* **109**, 053501 (2011).
- Miao, N. H., Sa, B. S., Zhou, J., Sun, Z. M. & Ahuja, R. Mechanical properties and electronic structure of the incompressible rhenium carbides and nitrides: A first-principles study. *Solid State Commun.* **151**, 1842–1845 (2011).
- Du, X. P., Lo, V. C. & Wang, Y. X. The Effect of Structure and Phase Transformation on the Mechanical Properties of Re₂N and the Stability of Mn₂N. *J. Comput. Chem.* **33**, 18–24 (2012).
- Zhang, R. F., Lin, Z. J., Mao, H. K. & Zhao, Y. S. Thermodynamic stability and unusual strength of ultra-incompressible rhenium nitrides. *Phys. Rev. B* **83**, 060101 (2011).
- Zang, C., Sun, H., Tse, J. S. & Chen, C. Indentation strength of ultraincompressible rhenium boride, carbide, and nitride from first-principles calculations. *Phys. Rev. B* **86**, 014108 (2012).
- Gu, Q., Krauss, G. & Steurer, W. Transition Metal Borides: Superhard versus Ultra-incompressible. *Adv. Mater.* **20**, 3620–3626 (2008).
- Zhao, E. J. & Wu, Z. J. Electronic and mechanical properties of 5d transition metal mononitrides via first principles. *J. Solid State Chem.* **181**, 2814–2827 (2008).
- Wang, Y. *et al.* Structural stability, phase transition, and mechanical and electronic properties of transition metal nitrides MN (M=Tc, Re, Os, and Ir): First-principles calculations. *Comput. Mater. Sci.* **56**, 116–121 (2012).
- Zhao, E. & Wu, Z. J. Structural, electronic and mechanical properties of ReN₂ from first principles. *Comput. Mater. Sci.* **44**, 531–535 (2008).
- Li, Y. L. & Zeng, Z. New potential super-incompressible phase of ReN₂. *Chem. Phys. Lett.* **474**, 93–96 (2009).
- Du, X. P., Wang, Y. X. & Lo, V. C. Investigation of tetragonal ReN₂ and WN₂ with high shear moduli from first-principles calculations. *Phys. Lett. A* **374**, 2569–2574 (2010).
- Kawamura, F., Yusa, H. & Taniguchi, T. Synthesis of rhenium nitride crystals with MoS₂ structure. *Appl. Phys. Lett.* **100**, 251910 (2012).
- Wang, Y. C., Yao, T. K., Yao, J. L., Zhang, J. W. & Gou, H. Y. Does the real ReN₂ have the MoS₂ structure? *Phys. Chem. Chem. Phys.* **15**, 183–187 (2013).
- Zhao, W. J., Xu, H. B. & Wang, Y. X. Prediction of a superhard material of ReN₄ with a high shear modulus. *Chin. Phys. B.* **19** (2010).
- Aydin, S., Ciftci, Y. O. & Tatar, A. Superhard transition metal tetranitrides: XN₄ (X=Re, Os, W). *J. Mater. Res.* **27**, 1705–1715 (2012).
- Ghosh, G., van de Walle, A. & Asta, M. First-principles calculations of the structural and thermodynamic properties of bcc, fcc and hcp solid solutions in the



- Al-TM (TM = Ti, Zr and Hf) systems: A comparison of cluster expansion and supercell methods. *Acta Mater.* **56**, 3202–3221 (2008).
31. Zhang, X. W., Trimarchi, G. & Zunger, A. Possible pitfalls in theoretical determination of ground-state crystal structures: The case of platinum nitride. *Phys. Rev. B* **79**, 092102 (2009).
 32. Zhang, M. G., Wang, H., Wang, H. B., Cui, T. & Ma, Y. M. Structural Modifications and Mechanical Properties of Molybdenum Borides from First Principles. *J. Phys. Chem. C* **114**, 6722–6725 (2010).
 33. Gregoryanz, E. *et al.* High P-T transformations of nitrogen to 170GPa. *J. Chem. Phys.* **126**, 184505 (2007).
 34. Pickard, C. J. & Needs, R. J. High-Pressure Phases of Nitrogen. *Phys. Rev. Lett.* **102**, 125702 (2009).
 35. Wang, X. *et al.* Cagelike Diamondoid Nitrogen at High Pressures. *Phys. Rev. Lett.* **109**, 175502 (2012).
 36. Wu, Z. J. *et al.* Crystal structures and elastic properties of superhard IrN₂ and IrN₃ from first principles. *Phys. Rev. B* **76**, 054115 (2007).
 37. Wessel, M. & Dronskowski, R. Nature of N-N Bonding within High-Pressure Noble-Metal Pernitrides and the Prediction of Lanthanum Pernitride. *J. Am. Chem. Soc.* **132**, 2421–2429 (2010).
 38. Kittel, C. *Introduction to solid state physics*. 4th edn, (Wiley, 1971).
 39. Chen, X. Q., Niu, H., Li, D. & Li, Y. Modeling hardness of polycrystalline materials and bulk metallic glasses. *Intermetallics* **19**, 1275–1281 (2011).
 40. Gao, F. M. *et al.* Hardness of covalent crystals. *Phys. Rev. Lett.* **91**, 015502 (2003).
 41. Šimůnek, A. & Vackář, J. Hardness of Covalent and Ionic Crystals: First-Principle Calculations. *Phys. Rev. Lett.* **96**, 085501 (2006).
 42. Li, K., Wang, X., Zhang, F. & Xue, D. Electronegativity Identification of Novel Superhard Materials. *Phys. Rev. Lett.* **100**, 235504 (2008).
 43. Lyakhov, A. O. & Oganov, A. R. Evolutionary search for superhard materials: Methodology and applications to forms of carbon and TiO₂. *Phys. Rev. B* **84**, 092103 (2011).
 44. Guo, X. *et al.* Hardness of covalent compounds: Roles of metallic component and *d* valence electrons. *J. Appl. Phys.* **104**, 023503–023507 (2008).
 45. Tian, Y., Xu, B. & Zhao, Z. Microscopic theory of hardness and design of novel superhard crystals. *Int. J. Refract. Met. Hard Mater.* **33**, 93–106 (2012).
 46. He, J., Wu, E., Wang, H., Liu, R. & Tian, Y. Ionicities of Boron-Boron Bonds in B₁₂ Icosahedra. *Phys. Rev. Lett.* **94**, 015504 (2005).
 47. Oganov, A. R. & Glass, C. W. Crystal structure prediction using *ab initio* evolutionary techniques: Principles and applications. *J. Chem. Phys.* **124**, 244704 (2006).
 48. Oganov, A. R., Lyakhov, A. O. & Valle, M. How Evolutionary Crystal Structure Prediction Works—and Why. *Acc. Chem. Res.* **44**, 227–237 (2011).
 49. Lyakhov, A. O., Oganov, A. R., Stokes, H. T. & Zhu, Q. New developments in evolutionary structure prediction algorithm USPEX. *Comput. Phys. Commun.* **184**, 1172–1182 (2013).
 50. Oganov, A. R., Ma, Y. M., Lyakhov, A. O., Valle, M. & Gatti, C. Evolutionary Crystal Structure Prediction as a Method for the Discovery of Minerals and Materials. *Rev. Mineral. Geochem.* **71**, 271–298 (2010).
 51. Kresse, G. & Furthmüller, J. Efficient iterative schemes for *ab initio* total-energy calculations using a plane-wave basis set. *Phys. Rev. B* **54**, 11169–11186 (1996).
 52. Kresse, G. & Joubert, D. From ultrasoft pseudopotentials to the projector augmented-wave method. *Phys. Rev. B* **59**, 1758–1775 (1999).
 53. Perdew, J. P., Burke, K. & Ernzerhof, M. Generalized Gradient Approximation Made Simple. *Phys. Rev. Lett.* **77**, 3865–3868 (1996).
 54. Togo, A., Oba, F. & Tanaka, I. First-principles calculations of the ferroelastic transition between rutile-type and CaCl₂-type SiO₂ at high pressures. *Phys. Rev. B* **78**, 134106 (2008).
 55. Togo, A., Oba, F. & Tanaka, I. Transition pathway of CO₂ crystals under high pressures. *Phys. Rev. B* **77**, 184101 (2008).
 56. Hill, R. The Elastic Behaviour of a Crystalline Aggregate. *Proc. Phys. Soc. London, Sect. A* **65**, 349 (1952).
 57. Segall, M. D. *et al.* First-principles simulation: ideas, illustrations and the CASTEP code. *J. Phys.-Condens. Mat.* **14**, 2717–2744 (2002).
 58. Segall, M. D., Shah, R., Pickard, C. J. & Payne, M. C. Population analysis of plane-wave electronic structure calculations of bulk materials. *Phys. Rev. B* **54**, 16317–16320 (1996).
 59. Vanderbilt, D. Soft self-consistent pseudopotentials in a generalized eigenvalue formalism. *Phys. Rev. B* **41**, 7892 (1990).

Acknowledgments

This work was supported by the National Basic Research Program of China (No. 2011CB808200), Program for Changjiang Scholars and Innovative Research Team in University (No. IRT1132), National Natural Science Foundation of China (Nos. 51032001, 11074090, 10979001, 51025206), and National Found for Fostering Talents of basic Science (No. J1103202). Parts of calculations were performed in the High Performance Computing Center (HPCC) of Jilin University.

Author Contributions

T.C. initiated the project. Z.Z. performed the first principle calculations and prepared all figures. Z.Z., K.B. and T.C. analyzed the data and wrote the manuscript text. D.L., D.D., F.T., X.J., C.C., X.H. and B.L. reviewed the manuscript.

Additional information

Supplementary information accompanies this paper at <http://www.nature.com/scientificreports>

Competing financial interests: The authors declare no competing financial interests.

How to cite this article: Zhao, Z.L. *et al.* Nitrogen concentration driving the hardness of rhenium nitrides. *Sci. Rep.* **4**, 4797; DOI:10.1038/srep04797 (2014).



This work is licensed under a Creative Commons Attribution-NonCommercial-ShareAlike 3.0 Unported License. The images in this article are included in the article's Creative Commons license, unless indicated otherwise in the image credit; if the image is not included under the Creative Commons license, users will need to obtain permission from the license holder in order to reproduce the image. To view a copy of this license, visit <http://creativecommons.org/licenses/by-nc-sa/3.0/>